


# A Progressive Build-up of Perineuronal Nets in the Somatosensory Cortex Is Associated with the Development of Chronic Pain in Mice

Giada Mascio,<sup>1</sup> Serena Notartomaso,<sup>1</sup> Katuscia Martinello,<sup>1</sup> Francesca Liberatore,<sup>1</sup> Domenico Bucci,<sup>1</sup> Tiziana Imbriglio,<sup>1</sup> Milena Cannella,<sup>1</sup> Nico Antenucci,<sup>2</sup> Pamela Scarselli,<sup>1</sup> Roberta Lattanzi,<sup>2</sup> Valeria Bruno,<sup>1,2</sup> Ferdinando Nicoletti,<sup>1,2</sup>  Sergio Fucile,<sup>1,2</sup> and Giuseppe Battaglia<sup>1,2</sup>

<sup>1</sup>Istituto di Ricovero e Cura a Carattere Scientifico Neuromed, Pozzilli, 86077, Italy, and <sup>2</sup>Department of Physiology and Pharmacology, Sapienza University, Rome, 00185, Italy

Chronic pain is sustained by a maladaptive form of neuronal plasticity occurring in all stations of the pain neuraxis, including cortical regions of the pain matrix. We report that chronic inflammatory pain induced by unilateral injection of complete Freund's adjuvant (CFA) in the hindpaw of male mice was associated with a progressive build-up of perineuronal nets (PNNs) in the contralateral somatosensory cortex (SSC), medial prefrontal cortex (mPFC), and reticular thalamic nucleus. In the SSC, the density of PNNs labeled by Wisteria floribunda agglutinin (WFA) was increased at both 3 and 7 d following CFA injection, but only after 7 d in the mPFC. The number of parvalbumin (PV)-positive interneurons enwrapped by WFA<sup>+</sup>/PNNs was also increased in all three brain regions of mice injected with CFA. Remarkably, PNN degradation induced by intracortical infusion of chondroitinase-ABC significantly reduced mechanical and thermal pain, and also reversed the increased frequency of IPSCs recorded in layer 5 pyramidal neurons of the contralateral SSC in CFA-injected mice. These findings suggest a possible relationship between cortical PNNs and nociceptive sensitization, and support the hypothesis that PNNs maintain their plasticity in the adult life and regulate cortical responses to sensory inputs.

**Key words:** chondroitinase ABC; chronic pain; inhibitory synaptic transmission; perineuronal nets; prefrontal cortex; somatosensory cortex

## Significance Statement

The brain extracellular matrix not only provides structural support, but also regulates synapse formation and function, and modulates neuronal excitability. We found that chronic inflammatory pain in mice enhances the density of perineuronal nets (PNNs) in the somatosensory cortex and medial prefrontal cortex. Remarkably, enzymatic degradation of PNNs in the somatosensory cortex caused analgesia and reversed alterations of inhibitory synaptic transmission associated with chronic pain. These findings disclose a novel mechanism of nociceptive sensitization and support a role for PNNs in mechanisms of neuronal plasticity in the adult brain.

## Introduction

Nociceptive sensitization reflects the development of a maladaptive form of neuronal plasticity occurring in all stations of the pain neuraxis, and aimed at increasing pain sensation and behavioral reactivity in response to sustained painful stimuli (Woolf

and Walters, 1991; Woolf, 1994, 2011; Woolf and Salter, 2000; Loretto and Woolf, 2009). The somatosensory cortex (SSC) has a key role in processing sensory-discriminative painful and nonpainful mechanical stimuli (Bushnell et al., 1999). In chronic pain, a more intense neuronal activation in the SSC and connected brain regions of the pain matrix contributes to the generation of allodynia, in which non-noxious tactile stimuli are perceived as painful (Komagata et al., 2011; Kim et al., 2012; Watanabe et al., 2015). The mechanisms underlying the SSC hyperexcitability in chronic pain are only partially elucidated. SSC excitability is regulated by several types of GABAergic inhibitory interneurons, which gate signal flow and sculpt network dynamics (Tremblay et al., 2016). In addition to pyramidal neurons (Eto et al., 2011; Kim and Nabekura, 2011), GABAergic interneurons are hyperactive in chronic pain. Using *in vivo* two-

Received Aug. 24, 2021; revised Jan. 19, 2022; accepted Jan. 21, 2022.

Author contributions: G.M., V.B., F.N., S.F., and G.B. designed research; G.M., S.N., K.M., F.L., D.B., T.I., and R.L. performed research; G.M., S.N., F.L., and G.B. wrote the first draft of the paper; S.N., K.M., F.L., D.B., T.I., M.C., N.A., P.S., and R.L. analyzed data; V.B., F.N., S.F., and G.B. edited the paper; V.B., F.N., S.F., and G.B. wrote the paper.

The authors declare no competing financial interests.

Correspondence should be addressed to Giuseppe Battaglia at giuseppe.battaglia@neuromed.it.

<https://doi.org/10.1523/JNEUROSCI.1714-21.2022>

Copyright © 2022 the authors

photon calcium imaging and electrophysiology, Eto et al. (2012) have found that responses of L2/3 GABAergic interneurons to sensory or electrical stimulation were enhanced in the complete Freund's adjuvant (CFA) mouse model of chronic inflammatory pain. This has been interpreted as a sterile adaptive response aimed at restraining an excessive activation of pyramidal neurons and the resulting increase in pain perception. The relative inefficiency of cortical GABAergic transmission in restraining nociceptive sensitization and the resulting reduction in pain threshold were ascribed to a downregulation of the  $K^+/Cl^-$  symporter, KCC2 (Eto et al., 2012), leading to a less hyperpolarizing GABA<sub>A</sub> receptor-mediated response (Rivera et al., 1999). Other mechanisms of plasticity involving cortical GABAergic interneurons remain unexplored.

Parvalbumin (PV)-expressing interneurons, which account for ~40% of cortical GABAergic interneurons and are involved in the generation of cortical network oscillations (Tremblay et al., 2016), are enwrapped by perineuronal nets (PNNs), specialized components of the extracellular matrix containing chondroitin sulfate proteoglycans, such as aggrecan, versican, neurocan, and brevican, linked to hyaluronic acid and tenascin-R (Takesian and Hensch, 2013; Testa et al., 2019). In the mouse SSC, PNNs appear after the first post-natal week, and their deposition coincides with the closure of critical windows of cortical plasticity (Pizzorusso et al., 2002; Miyata et al., 2012; Takesian and Hensch, 2013). PNNs restrain the plasticity of PV<sup>+</sup> interneurons and contribute to consolidate neuronal circuitries around PV<sup>+</sup> interneurons (Takesian and Hensch, 2013). Abnormalities in PNNs have been associated with neurodevelopmental disorders, such as schizophrenia (Berretta, 2012; Berretta et al., 2015).

Although PNNs have been linked to processes of developmental plasticity, their dynamic function is maintained in the adult life. Even once established, PNNs may disassemble and assemble in response to stress or during learning (Beurdeley et al., 2012; Sorg et al., 2016). PNNs have been associated to maladaptive forms of neuronal plasticity, as occurs in drug addiction. For example, removing PNNs in the prefrontal cortex (PFC) impairs the acquisition of memories associated with cocaine (Slaker et al., 2015), and removing PNNs in the amygdala restrains cocaine and heroin relapse in rats (Xue et al., 2014). To our knowledge, PNNs have never been studied in models of chronic pain, although changes in PNNs have been associated with pain in mouse models of multiple sclerosis and traumatic brain injury (Potter et al., 2016; Hsieh et al., 2017).

We now report that chronic inflammatory pain induced by unilateral CFA injection in the plantar surface of the hindpaw in mice progressively enhanced PNN deposition in the contralateral SSC, PFC, and reticular thalamic nucleus (RTN), and this was associated with increased synaptic inhibition of layer 5 (L5) pyramidal neurons in the SSC. Remarkably, enzymatically induced degradation of PNNs in the contralateral SSC reduced mechanical and thermal pain, suggesting a causal link between PNNs and the development of nociceptive sensitization in the SSC.

## Materials and Methods

**Animals.** All experiments were conducted according to the European (86/609/EEC) and Italian (D. Lgs. 26/2014) guidelines of animal care. The experimental protocol was approved by the Italian Ministry of Health (1135/2020-PR). All efforts were made to minimize animal suffering and the number of animals used. In most of the experiments, we used adult male C57BL/6J mice (20–25 g, body weight) purchased from

Charles River. All mice were housed under a standard 12/12 h light/dark cycle with food and water *ad libitum*.

**Experimental paradigm.** Initially, we used two groups of 6 mice unilaterally injected with either vehicle or CFA in the hindpaw to assess mechanical pain thresholds at 3 and 7 d after CFA injection. Two groups of CFA-injected mice (4 mice per group) were used for immunofluorescent staining of Wisteria floribunda agglutinin (WFA)<sup>+</sup> PNNs in the SSC and mPFC at 3 and 7 d after CFA injection. Only one group of 4 mice injected with vehicle and killed at 7 d was used as a control. Two groups of 5 mice treated with vehicle and two groups of 5 mice treated with CFA were used for immunofluorescent staining or stereological counting of WFA<sup>+</sup> PNNs in the S1HL (hindlimb SSC1) at 7 d. Two groups of 3 or 4 mice treated with either vehicle or CFA were used for stereological WFA<sup>+</sup> PNN counting in the mPFC at 7 d. Two groups of 4 mice treated with vehicle and two groups of 4 mice treated with CFA were used for immunofluorescent staining of WFA<sup>+</sup> PNNs in the RTN. Two groups of 8 mice treated with either vehicle or CFA and killed at 3 d were used for the analysis of transcripts encoding structural components of PNNs or PNN-degrading enzymes in the SSC. Four groups of 5 mice injected with either vehicle or CFA and killed at 7 d were used for electrophysiological analysis in the SSC. Fifty CFA-injected mice were locally infused with either vehicle ( $n = 25$ ) or the PNN-degrading enzyme chondroitinase-ABC (ChABC) ( $n = 25$ ) in the SSC after 4 d. These mice were used for (1) assessment of mechanical pain thresholds and thermal latencies at days 4 and 7 following CFA injection, (2) immunofluorescent staining of WFA<sup>+</sup> PNNs, and (3) electrophysiological analysis in the SSC at 7 d after CFA injection corresponding to 3 d after ChABC or vehicle infusion. Twenty-one naive mice were locally infused with either vehicle ( $n = 10$ ) or ChABC ( $n = 11$ ) in the SSC and used for assessment of mechanical pain thresholds or thermal latencies before infusions and 3 d later.

**Induction of chronic inflammatory pain.** Tissue inflammation was induced by subcutaneous injections of 20  $\mu$ l of CFA (1 mg/ml, #F5881 Sigma-Aldrich) in the plantar surface of the right hindpaw; control mice were injected subcutaneously with Incomplete Freund's Adjuvant (Vehicle, #F5506 Sigma-Aldrich) in the right hindpaw.

**Pain testing/von Frey hair assay.** The von Frey hair assay was used to measure mechanical pain thresholds. Animals were placed in transparent Plexiglas boxes over a screen that allowed access to the paws. Before the start of testing, all mice underwent a period of habituation to the boxes (5–10 min/day, for 3 d before baseline testing). Mice were also habituated for 5–10 min in the testing boxes at the start of each test day. After this period, the plantar surface of each hindpaw was stimulated  $\times 5$  with a weighted von Frey hair monofilament. An observer blinded to the experimental/treatment groups monitored and recorded behavioral responses to stimulation. Hindpaw stimulation was repeated through a progressive series of filament weights (0.04–2.0 g). Left and right paw responses were averaged within each animal to provide a combined threshold for each test day, and these combined thresholds were used for subsequent analysis. Mice were tested on days 3 and 7.

**Pain testing/thermal assay.** The hot plate test was used to measure thermal pain threshold. Mice were placed on a 50°C heated surface (Ugo Basile); the time to the first sign of nociception, such as licking of the back paws or jumping, was recorded; and the animal was immediately removed. Mice were tested before CFA (baseline) and 3 and 7 d after CFA.

**Enzymatic degradation of PNNs in the SSC.** Protease-free ChABC (Sigma-Aldrich) was dissolved to 50 U/ml in PBS containing 0.1% BSA and filtered through a 0.2  $\mu$ m filter. Injections (0.5  $\mu$ l each at 0.1  $\mu$ l/min) were performed stereotaxically under isoflurane anesthesia with a 1  $\mu$ l Hamilton syringe and a 33 gauge needle at the following three sites in the SSC contralateral with respect to CFA injection (in mm from bregma and the surface of the dura mater): (1) AP: 1; lateral: 2.7; vertical: 2.5; (2) AP: 0; lateral: 3; vertical: 2.2; (3) AP: -1; lateral: 3; vertical: 2 (Paxinos and Franklin, 2001). Control mice were infused with vehicle (PBS containing 0.1% BSA). After each injection, the needle was left *in situ* for additional 2 min before being withdrawn.

**Immunofluorescent staining of WFA<sup>+</sup> PNNs.** Brain sections were stained with WFA, a lectin that binds selectively N-acetylglactosamine-



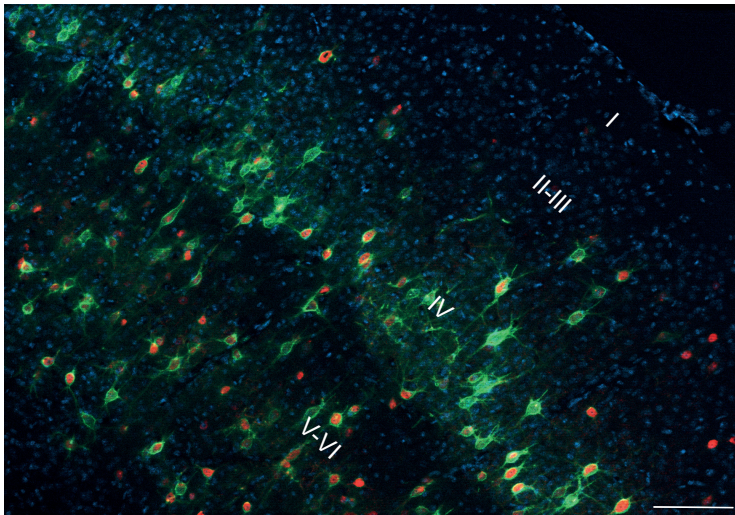


**Figure 1.** Representative image of WFA<sup>+</sup> PNNs in the SSC. Green represents WFA<sup>+</sup> PNNs. Red represents PV staining. Blue represents DAPI-stained cell nuclei. This image was obtained with a Carl Zeiss Apotome confocal microscope. I, II, III, IV, V and VI represent cortical layers. Scale bar, 50  $\mu$ m.

$\beta$ 1 residues of glycoproteins within the extracellular matrix. WFA fluorescent staining was performed using biotin-conjugate WFA (1:500; #L1516, Sigma-Aldrich; RRID:AB\_2620171) and fluorescent secondary antibody (Streptavidin AlexaFluor-488, 1:200, Invitrogen). We also performed double immunofluorescent staining for WFA and PV (monoclonal rabbit anti-PV antibodies; 1:1000, #PV27, Swant; RRID:AB\_2631173) using secondary AlexaFluor-488 antibody (1:200, Jackson ImmunoResearch Laboratories) and donkey anti rabbit Cy3 secondary antibody (1:200, Jackson ImmunoResearch Laboratories). Sections were examined with a Carl Zeiss 780 confocal laser scanning microscope and processed with ZEN software and/or LAS X software or with a Carl Zeiss Apotome confocal laser scanning microscope. Cell counting was performed in coronal sections at 10 $\times$  magnification.

**Stereological counting of WFA<sup>+</sup> PNNs in the SSC and PFC.** Mice were killed and brains were fixed in Carnoy's solution (ethanol 60%, acetic acid 10%, and chloroform 30%), and included in paraffin. Tissue sections (20  $\mu$ m) were incubated overnight with biotin-conjugated WFA (1:500, #L1516, Sigma-Aldrich). For detection, 3,3'-diaminobenzidine tetrachloride (Millipore-Sigma) was used. The number of WFA<sup>+</sup> PNNs in the SIHL region of the SSC and mPFC (containing cingulate cortex area 1, prelimbic and infralimbic cortex) was assessed by stereological technique and optical fractionator using a Carl Zeiss Axio Imager M1 microscope equipped with a motorized stage, a focus control system (Zeta axis), and a digital video camera. The software Image-Pro Plus 6.2 for Windows (Media Cybernetics) equipped with a Macro was used for the analysis of digital images. The Macro was obtained by Imagine and Computer. For the SIHL, the analysis was performed on four sections of 20  $\mu$ m, sampled every 180  $\mu$ m in the rostrocaudal extension of the SSC using a grid of disectors with a counting frame of 50  $\times$  50  $\mu$ m, and a grid size (distance between disectors center to center) of 300  $\times$  300  $\mu$ m. For the mPFC, the analysis was performed on three sections of 20  $\mu$ m, sampled every 200  $\mu$ m in the rostrocaudal extension of the mPFC using a grid of disectors with a counting frame of 40  $\times$  40  $\mu$ m, and a grid size (distance between disectors center to center) of 200  $\times$  200  $\mu$ m. The total number of WFA<sup>+</sup> PNNs was computed according to the formula:  $N = \Sigma(n) \times 1/SSF \times 1/ASF \times 1/TSF$ , where  $n$  is the total number of cells counted on each disector, SSF (fraction of sections sampled) is the number of regularly spaced sections used for counts divided by the total number of sections across the areas, ASF (area sampling frequency) is the disectors area divided by the area between disectors (disector area  $\times$  disectors number/region area), and TSF (thickness sampling frequency) is the disector thickness divided by the section thickness. The Cavalieri estimator method was used to evaluate the volume of the SSC.

**Gene expression analysis.** Mice were killed and the brains were removed, and the SSC was dissected and frozen on liquid nitrogen. Total

RNA was extracted using the Trizol reagent (Invitrogen) according to the manufacturer's instructions. The RNA was further treated with DNase (QIAGEN), and single-strand cDNA was synthesized from 1.5  $\mu$ g of total RNA using Superscript III (Invitrogen) and random hexamers. Real-time PCR was performed on 15 ng of cDNA by using specific primers and Power SYBR Green Master Mix (Bio-Rad) on an Applied Biosystems Step-One instrument. Thermal cyclers conditions were as follows: 10 min at 95 $^{\circ}$ C, 40 cycles of denaturation (15 s at 95 $^{\circ}$ C), and combined annealing/extension (1 min at 58 $^{\circ}$ C–60 $^{\circ}$ C). mRNA copy number for each gene was calculated from serially diluted standard curves simultaneously amplified with the samples and normalized with respect to the GAPDH mRNA copy number using the following formula:  $(X \text{ mRNA}/\text{GAPDH mRNA}) \times 10^6$ . Each sample was analyzed in duplicate together with two negative controls. We used the following primers: Nptx2 forward 5'AGCTCCGCACAAATGTGTCT-3', reverse 5'GAATGCACTGTTGCCTCGCT-3'; Npas4 forward 5'ACACTCGCAA GGGTGTCTTC-3' reverse 5'GCAACCAGGTCCACC ATAGA-3'; Mmp9 forward 5'CCAGCCGACTTTTG TGGTCT-3' reverse 5'-TGGCCTTTAGTGTCTGGC TG-3'; Bcan forward 5'TCAAAGGGGTCTCTTC CTC-3' reverse 5'ATCCATGTCTCCAGAGCAGG-3'; Vcan forward 5'GGATCATCTGGATGGCGATGT-3', reverse 5'AG CCGTAATCGCATTGGTCA-3'; Tnr forward 5'CCTACCAGCT GCTGTTTCGT-3', reverse 5'-AGTTGATGCAGACACCCAGG-3'; Adam forward 5'TGGACACGGGAATGTTTGAT-3', reverse 5'-AGTACATGTGCTGGTGCAT-3'; Hapln1 forward 5'TCCCTGGTC ATCAGGATCT-3', reverse 5'ATTGAGCTCCAGTCGTG-3'; Acan forward 5'GATACTCTGACATTTGAGG-3', reverse 5'GTA TCTGACGGTCTGGTCT-3'; Pv forward 5'GCTTCTCTCAGATG CCAGA-3', reverse 5'CCACTTAGCTTTCAGCCACC-3'; Sst forward 5'CCTGCGACTAGACTGACCA-3', reverse 5'CCAGTTCCTGTT TCCCGGTG-3'; Gad1 forward 5'GTACTCTGTGACAGAGCCG-3', reverse 5'GTATTAGGATCCGCTCCCGC-3'; Gad2 forward 5'GGCTC TGGCGATGGAATCTT-3', reverse 5'-TGGAAATCATTTTCCCTCTC TCG-3'; Gat1 forward 5'CACCATCCCAGGACTTTCCTC-3', reverse 5'GGGACACCAGAACAGAGTGG-3'; and GAPDH forward 5'-CGTCCCCTAGACAAAATGGT-3', reverse 5'-TCAATGAAGGGG TCGTTGAT-3'.

**Whole-cell recordings from L5 in the primary SSC.** Coronal slices, 350  $\mu$ m in thickness, were cut in glycerol-based ACSF with a vibratome (Leica Microsystems, VT 1000S) immediately after surgical resection. Slices were placed in a slice incubation chamber at room temperature with oxygenated ACSF and transferred to a recording chamber within 1–6 h after slice preparation. Spontaneous IPSCs (sIPSCs) were recorded from L5 pyramidal neurons in the ipsilateral and contralateral SSC 7 d after CFA or vehicle injection. In a subset of experiments, recordings were performed 4 d after intracortical infusion of vehicle or ChABC (corresponding to 7 d after CFA injection, see above). All recordings were performed at 22 $^{\circ}$ C–25 $^{\circ}$ C and  $-70$  mV holding potential using a Multiclamp 700A amplifier (Molecular Devices; no liquid junction correction; 10 kHz sampling rate, 2 kHz low pass filter applied), in the presence of CNQX (20  $\mu$ M) and D-AP5 (40  $\mu$ M) to block AMPA receptors and kainate receptors, respectively. ACSF had the following composition: 125 mM NaCl, 2.5 mM KCl, 2 mM CaCl<sub>2</sub>, 1.25 mM NaH<sub>2</sub>PO<sub>4</sub>, 1 mM MgCl<sub>2</sub>, 26 mM NaHCO<sub>3</sub>, 10 mM glucose, pH 7.35. Glycerol-based ACSF solution contained 250 mM glycerol, 2.5 mM KCl, 2.4 mM CaCl<sub>2</sub>, 1.2 mM MgCl<sub>2</sub>, 1.2 mM NaH<sub>2</sub>PO<sub>4</sub>, 26 mM NaHCO<sub>3</sub>, 11 mM glucose, pH 7.35. Patch pipettes were filled with 140 mM KCl, 10 mM HEPES, 5 mM BAPTA, 2 mM MgCl<sub>2</sub>, and 2 mM Mg-ATP, pH 7.35, with KOH. All drugs were purchased from Sigma-Aldrich, with the exception of AP5 and CNQX, which were purchased from Tocris Cookson and freshly prepared before the experiments. sIPSC analysis was performed with Clampfit 10 software (Molecular Devices; for details see Martinello et al., 2018).

**sIPSC analysis.** sIPSC kinetic analysis was performed with Clampfit 10 software (Molecular Devices), as in Martinello et al. (2018), by using

a template-based detection algorithm. The rise time was estimated as the time taken by the current to increase from 10% to 90% of the peak and the decay time as the time taken by the current to decrease from 90% to 10%. The inhibitory charge of a single synaptic event (Q) was measured as the time integral of the spontaneous GABA<sub>A</sub>-mediated synaptic currents.

**Statistical analysis.** Statistical analysis was performed by Student's *t* test (see Figs. 3B,D, 4D), two-way ANOVA + Fisher's LSD (see Figs. 2B–D, 4B, 5B, 6, 7B, 8E,F; Extended Data Figs. 6–1, 8–1B–E,G–I,L), or two-way ANOVA for repeated measures + Fisher's LSD (see Fig. 7C–F). Statistical significance was set at  $p < 0.05$ . In Figure 8C, D and Extended Data Figure 8–1A, F, statistical significance of cumulative distributions of amplitudes and interevent intervals was assessed using the Kolmogorov–Smirnov test with a Clampfit 10 software.

## Results

### Progressive build-up of PNNs in the SSC, mPFC, and RTN of mice developing chronic inflammatory pain

Unilateral CFA injection into the hindpaw caused a substantial reduction in mechanical pain thresholds at both 3 and 7 d with no difference between the two time points. In mice injected with vehicle, thresholds did not differ between 3 and 7 d (mean  $\pm$  SEM: vehicle 3 d,  $0.78 \pm 0.11$ ; vehicle 7 d,  $0.95 \pm 0.16$ ; CFA 3 d,  $0.10 \pm 0.03$ ; CFA 7 d,  $0.082 \pm 0.02$ ; statistical analysis: time,  $F_{(1,10)} = 0.4362$ ;  $p = 0.5239$ ; treatment,  $F_{(1,10)} = 75.74$ ;  $p < 0.0001$  interaction,  $F_{(1,10)} = 0.5328$ ;  $p = 0.4822$ ). For this reason, we used a single group of controls (7 d after vehicle injection) for the analysis of PNNs in mice developing chronic inflammatory pain.

We measured the density of cells enwrapped by PNNs in the SSC, mPFC, and RTN after fluorescent staining with WFA. Figure 1 shows a representative image of WFA<sup>+</sup> PNNs (green) and PV<sup>+</sup> interneurons (red) in the SSC of control mice, where ~75% of WFA<sup>+</sup> PNNs enwrapped PV<sup>+</sup> interneurons, and 20–25% of PV<sup>+</sup> interneurons were not WFA-positive.

PNNs were examined in three sections of the SSC (AP: 0.98, 0.02, and –1.06 mm from bregma). An increased density of WFA<sup>+</sup> PNNs was found in the contralateral SSC at 3 and 7 d after CFA injection compared with the ipsilateral cortex and both cortices of vehicle-injected mice. The increase was significant at both time points but was more prominent at 7 d (AP 0.98 mm: treatment,  $F_{(2,18)} = 39.54$ ;  $p < 0.0001$ ; cortical side,  $F_{(1,18)} = 108.1$ ;  $p < 0.0001$ ; interaction,  $F_{(2,18)} = 18.75$ ;  $p < 0.0001$ ; AP 0.02 mm: treatment,  $F_{(2,18)} = 3.683$ ;  $p = 0.0456$ ; cortical side,  $F_{(1,18)} = 14.95$ ;  $p = 0.0011$ ; interaction,  $F_{(2,18)} = 4.493$ ;  $p = 0.0261$ ; AP –1.06 mm: treatment,  $F_{(2,18)} = 16.74$ ;  $p < 0.0001$ ; cortical side,  $F_{(1,18)} = 30.96$ ;  $p < 0.0001$  interaction,  $F_{(2,18)} = 13.21$ ;  $p = 0.0003$ )

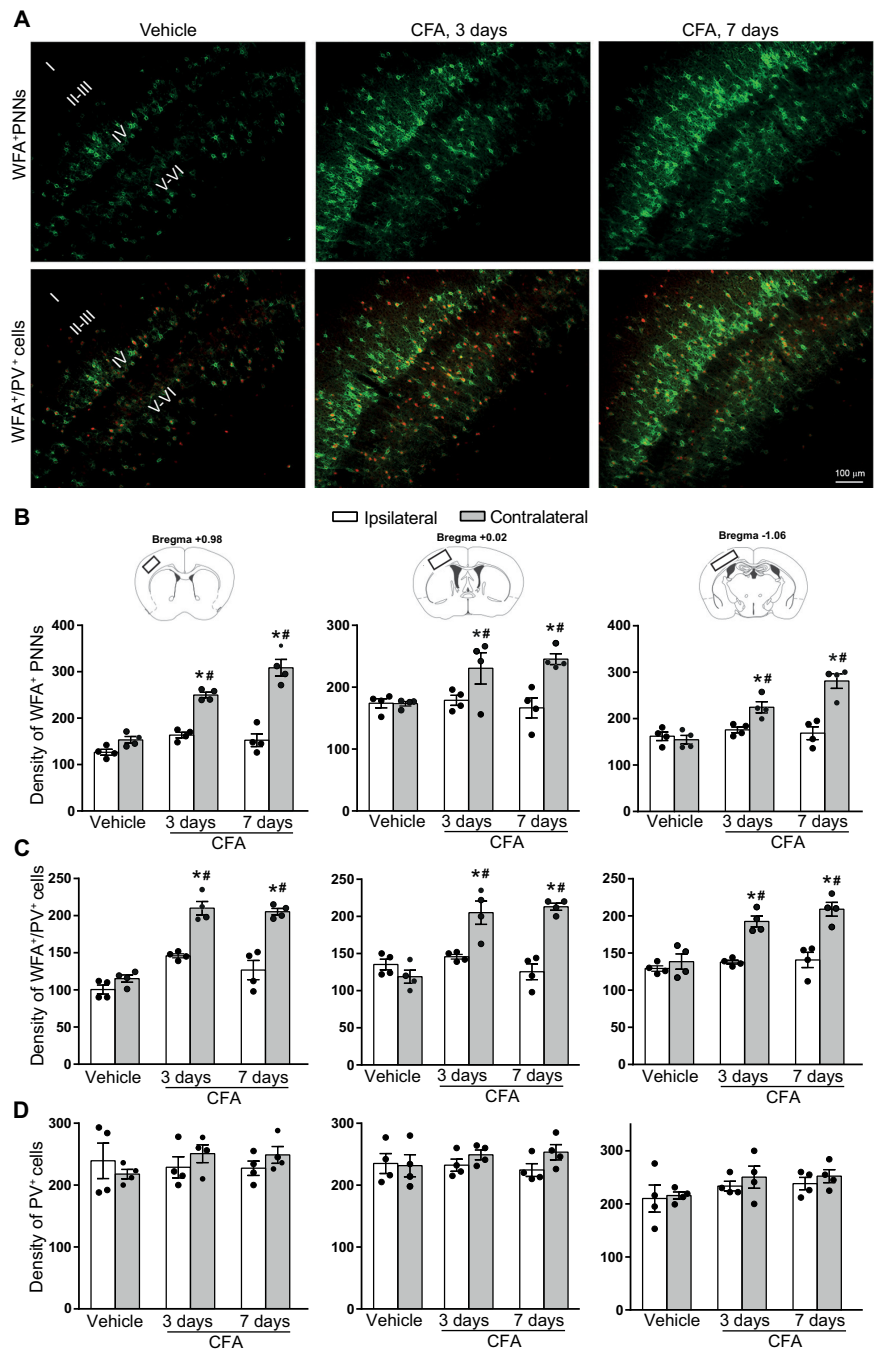


**Figure 2.** Increased density of WFA<sup>+</sup> PNNs in the SSC of mice developing chronic inflammatory pain. **A**, Representative immunofluorescent staining of WFA<sup>+</sup> PNNs (green) and PV<sup>+</sup> neurons (red) in the contralateral SSC of mice injected with vehicle (7 d) or CFA (3 or 7 d). I, II, III, IV, V and VI represent cortical layers. **B–D**, Density of WFA<sup>+</sup> PNNs, WFA<sup>+</sup> PNN-enwrapped PV<sup>+</sup> interneurons, or PV<sup>+</sup> interneurons in the ipsilateral and contralateral SSC of mice injected with vehicle or CFA. Values are mean  $\pm$  SEM of 4 mice per group. Significantly different versus the respective values obtained in the ipsilateral SSC (\*) or the respective mice treated with vehicle (#).

(Fig. 2A,B). The density of WFA<sup>+</sup>/PV<sup>+</sup> cells was also increased in the contralateral SSC of CFA-injected mice (AP 0.98 mm: treatment,  $F_{(2,18)} = 49.34$ ;  $p < 0.0001$ ; cortical side,  $F_{(1,18)} = 73.81$ ;  $p < 0.0001$  interaction,  $F_{(2,18)} = 9.656$ ;  $p = 0.0014$ . AP 0.02 mm: treatment,  $F_{(2,18)} = 16$ ;  $p = 0.0001$ ; cortical side,  $F_{(1,18)} = 32.61$ ;  $p < 0.0001$ ; interaction,  $F_{(2,18)} = 16.68$ ;  $p < 0.0001$ ; AP –1.06 mm: treatment,  $F_{(2,18)} = 14.88$ ;  $p = 0.0002$ ; cortical side,  $F_{(1,18)} = 47.27$ ;  $p < 0.0001$ ; interaction,  $F_{(2,18)} = 7.748$ ;  $p = 0.0037$ ) (Fig. 2C). Comparative analysis of Figure 2B, C showed that, at 3 d,



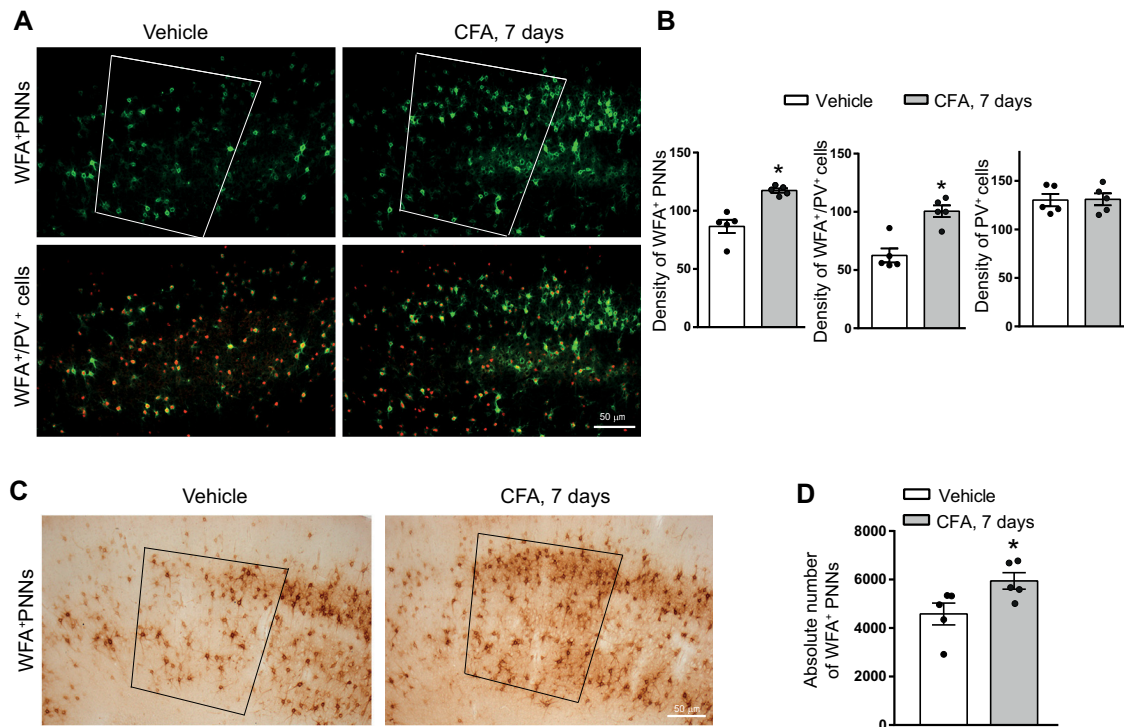


**Figure 3.** Increased density and absolute number of WFA<sup>+</sup> PNN in the SHL1 region of the contralateral SSC of mice developing chronic inflammatory pain. **A**, Representative immunofluorescent staining of WFA<sup>+</sup> PNNs (green) and PV<sup>+</sup> neurons (red) in the SHL1 region of the contralateral SSC of mice injected with CFA or vehicle, **B**, Density of WFA<sup>+</sup> PNNs, WFA<sup>+</sup> PNN/PV<sup>+</sup> cells, and PV<sup>+</sup> cells in the contralateral SHL1 region. Values are mean ± SEM of 5 mice per group. \*Significantly different versus the respective values obtained in mice treated with vehicle. **C**, DAB staining used for stereological cell counting. **D**, The absolute number of WFA<sup>+</sup> PNNs in the contralateral S1HL. Values are mean ± SEM of 5 mice per group. \*Significantly different versus the values obtained in mice treated with vehicle.

WFA<sup>+</sup>/PV<sup>+</sup> cells largely accounted for the increase in the total density of WFA<sup>+</sup> PNNs in the two most anterior sections of the contralateral SSC of CFA-injected mice (% WFA<sup>+</sup>/PV<sup>+</sup> cells with respect to total WFA<sup>+</sup> PNNs: AP 0.98 = 84% vs 76%; AP 0.02 = 89% vs 69%; AP -1.06, and 85% vs 88% in CFA- vs vehicle-injected mice, respectively). A greater percentage of WFA<sup>+</sup>/PV<sup>+</sup> cells was only observed in the midsection of the contralateral SSC of CFA-injected mice at 7 d (% WFA<sup>+</sup>/PV<sup>+</sup> cells with respect to total WFA<sup>+</sup> PNNs: AP 0.98 = 67% vs 76%; AP 0.02 = 87% vs 69%; AP -1.06 = 74% vs 88% in CFA- vs vehicle-injected mice, respectively). The total density of PV<sup>+</sup> interneurons was unchanged in response to CFA-induced inflammatory pain (Fig. 2D). Measurements of the transcripts encoding PV, somatostatin, GAD-67 (GAD1), GAD-65 (GAD2), and GAT-1 showed no changes between saline and CFA-injected mice in the SSC. There was only an unexpected difference in PV mRNA levels between the ipsilateral and contralateral SSC of vehicle-injected mice (treatment,  $F_{(1,16)} = 0.07, 114; p = 0.7931$ ; cortical side,  $F_{(1,16)} = 4.865; p = 0.0424$  interaction,  $F_{(1,16)} = 3.57; p = 0.0771$ ) (Extended Data Fig. 6-1).

An increase in the density of WFA<sup>+</sup> PNNs ( $t_{(8)} = 5.146; p = 0.0009$ ) and WFA<sup>+</sup>/PV<sup>+</sup> cells ( $t_{(8)} = 4.869; p = 0.0012$ ) could also be detected in the S1HL portion of contralateral SSC, which receives sensory inputs from the CFA-injected hindlimbs (Fig. 3A,B). Here, WFA<sup>+</sup>/PV<sup>+</sup> cells largely accounted for the increase in the total density of WFA<sup>+</sup> PNNs in CFA-injected mice at 7 d (% WFA<sup>+</sup>/PV<sup>+</sup> cells with respect to total WFA<sup>+</sup> PNNs: 86% vs 72% in CFA- vs vehicle-injected mice, respectively). To confirm these findings using an unbiased method of detection, we performed a stereological counting of WFA<sup>+</sup> cells in the whole contralateral S1HL cortex after DAB staining. The absolute number of WFA<sup>+</sup> cells was significantly enhanced in the contralateral

S1HL cortex 7 d after CFA injection ( $t_{(8)} = 2412; p = 0.0212$ ) (Fig. 3C,D).

In the contralateral mPFC, including the anterior cingulate, prelimbic, and infralimbic cortices, the density of WFA<sup>+</sup> PNNs (treatment,  $F_{(2,18)} = 22.18; p < 0.0001$ ; cortical side,  $F_{(1,18)} = 15.24; p = 0.001$ ; interaction,  $F_{(2,18)} = 13.93; p = 0.0002$ ) and WFA<sup>+</sup>/PV<sup>+</sup> cells (treatment,  $F_{(2,18)} = 11.24; p = 0.0007$ ; cortical side,  $F_{(1,18)} = 11.41; p = 0.0034$ ; interaction,  $F_{(2,18)} = 18.36; p < 0.0001$ ) was largely increased 7 d after CFA injection. No significant changes were detected at 3 d (Fig. 4A,B). The percentage of WFA<sup>+</sup>/PV<sup>+</sup> cells with respect to total WFA<sup>+</sup> PNNs was similar in CFA- and vehicle-injected mice at 7 d (93% and 90%, respectively). The increase in WFA<sup>+</sup>/PNN<sup>+</sup> cells was confirmed by stereological counting ( $t_{(5)} = 2.902; p = 0.0169$ ) (Fig. 4C,D).

A significant increase in the density of WFA<sup>+</sup> PNNs and WFA<sup>+</sup>/PV<sup>+</sup> cells was found in the contralateral RTN 7 d following CFA injection. WFA<sup>+</sup>/PV<sup>+</sup> cells were 85% of total WFA<sup>+</sup> PNNs in the contralateral RTN of vehicle-injected mice, and this number increased to 95% in CFA-injected mice. No changes in WFA<sup>+</sup> PNN and WFA<sup>+</sup>/PV<sup>+</sup> density were found in the ipsilateral RTN after CFA injection (treatment,  $F_{(1,12)} = 25.48; p = 0.0003$ ; side,  $F_{(1,12)} = 10.96; p = 0.0062$ ; interaction,  $F_{(1,12)} = 13.56; p = 0.0031$ ) (Fig. 5A,B).

Thus, the build-up of PNNs in response to chronic pain was observed in more than one region of the pain matrix.

### Changes in the expression of genes involved in the formation or degradation of PNNs in the SSC of mice with chronic inflammatory pain

To shed light onto the mechanisms by which chronic pain caused an increased density of PNNs in the contralateral SSC, we

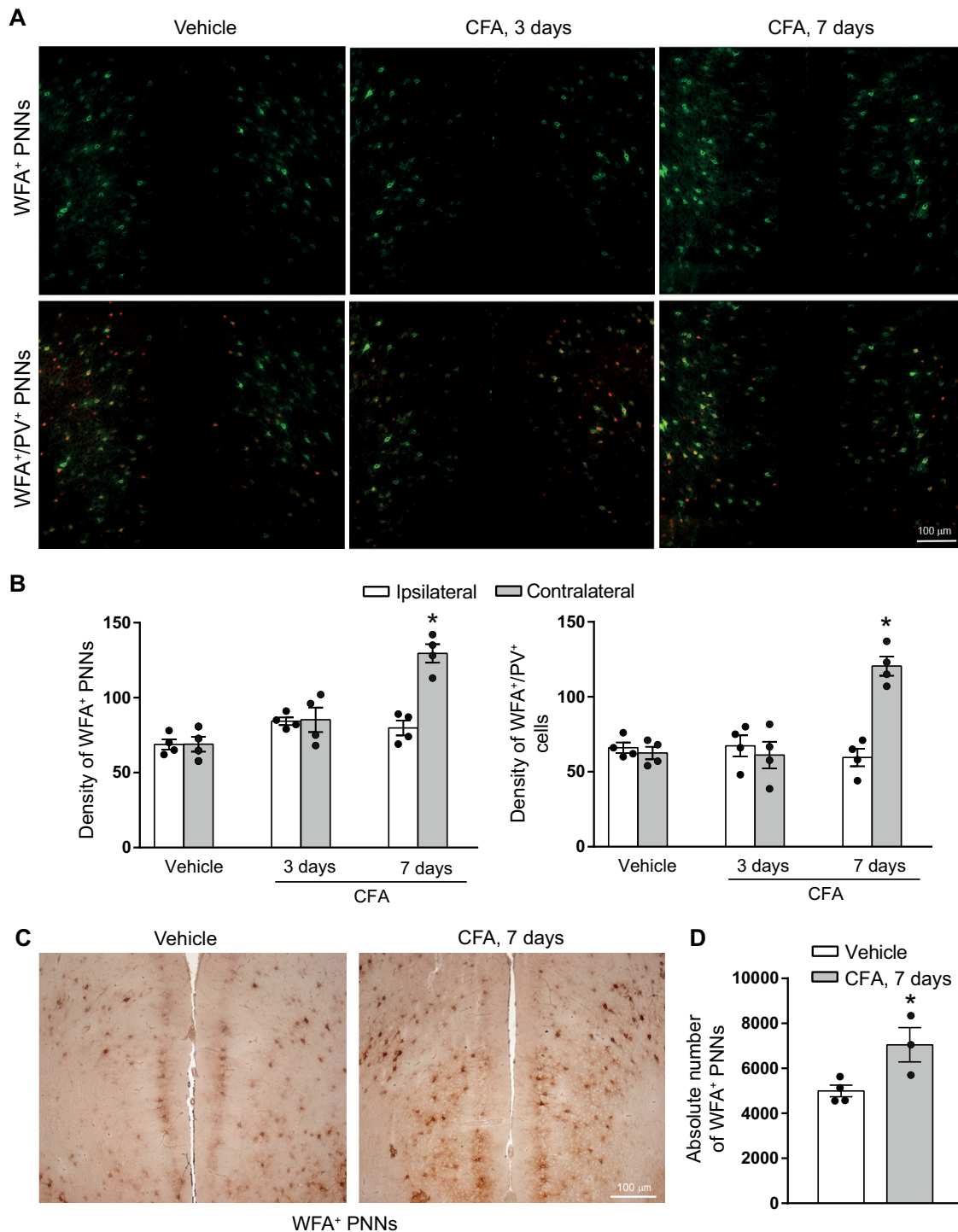


**Figure 4.** Increased density and absolute number of WFA<sup>+</sup> PNN in the contralateral mPFC 7 d after CFA injection in mice. **A**, Representative immunofluorescent staining of WFA<sup>+</sup> PNN (green) and PV<sup>+</sup> neurons (red) in the mPFC of mice injected with CFA (3 or 7 d) or vehicle (7 d). **B**, Density of WFA<sup>+</sup> PNNs and WFA<sup>+</sup>/PV<sup>+</sup> cells. Values are mean ± SEM of 4 mice per group. \*Significantly different versus all other values. **C**, DAB staining used for stereological cell counting. **D**, The absolute number of WFA<sup>+</sup> PNNs in the contralateral mPFC. Values are mean ± SEM of 3 or 4 mice per group. \*Significantly different versus vehicle.

measured the transcripts of a number of proteins involved in the formation or degradation of PNNs. The analysis was restricted to the ipsilateral and contralateral SSC of CFA or saline-injected mice at 3 d after injection, when the build-up of PNNs was ongoing. We examined the transcripts of the following genes: Acan, Bcan, and Vcan, encoding the chondroitin sulfate proteoglycans, aggrecan, brevican, and versican, respectively; Tnr, encoding tenascin-R; Nptx2, encoding the neuronal activity-

regulated protein, pentraxin or Narp; Npas4, encoding the homonymous activity-dependent transcription factor; Adamts1, encoding ADAMTS1; Hapln1, encoding the hyaluronan and proteoglycan link protein 1; and mmp9 encoding the PNN-degrading enzyme, matrix metalloproteinase 9 (MMP-9). The transcripts encoding tenascin-R (treatment,  $F_{(1,27)} = 0.1913$ ;  $p = 0.6653$ ; cortical side,  $F_{(1,27)} = 2.208$ ;  $p = 0.1489$ ; interaction,  $F_{(1,27)} = 2.712$ ;  $p = 0.1112$ ) and NPTX2 (treatment,  $F_{(1,28)} =$

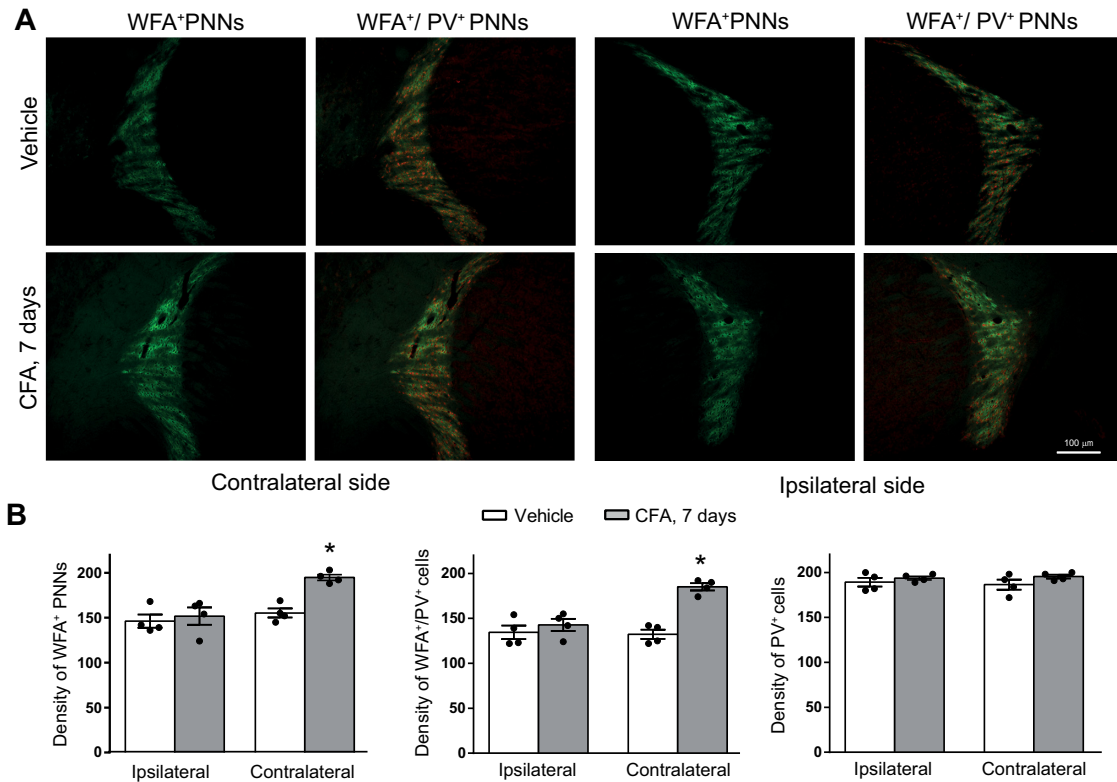


**Figure 5.** Increased density of WFA<sup>+</sup> PNN in the contralateral RTN 7 d after CFA injection in mice. **A**, Representative immunofluorescent staining of WFA<sup>+</sup> PNNs (green) and PV<sup>+</sup> neurons (red) in the RTN of mice injected with CFA or vehicle. **B**, Density of WFA<sup>+</sup> PNNs, WFA<sup>+</sup>/PV<sup>+</sup> cells, and PV. Values are mean ± SEM of 4 mice per group. \*Significantly different versus all other values.

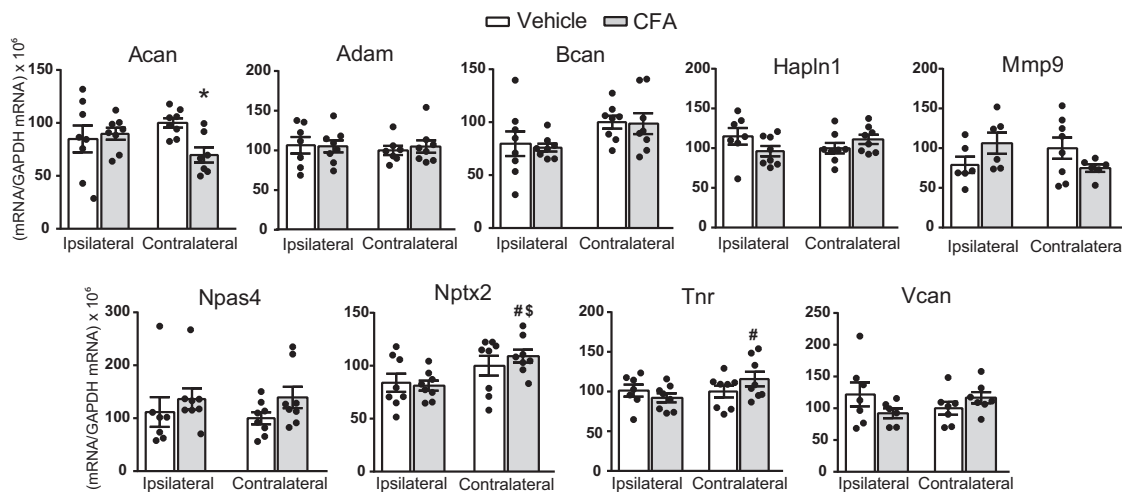


**Figure 6.** Expression of genes encoding structural proteins or degrading enzymes of PNNs in the SSC of mice developing chronic inflammatory pain. mRNA values were measured in the ipsilateral and contralateral SSC 3 d after unilateral injection of CFA or vehicle. Values are mean ± SEM of 6-8 determinations per group. Significant difference versus the respective values obtained in the contralateral SSC of mice treated with vehicle (\*), the ipsilateral SSC of mice treated with CFA (#), or the ipsilateral SSC of mice treated with vehicle (\$). The expression of genes encoding protein markers of GABAergic interneurons in the SSC of mice developing chronic inflammatory pain is reported in Extended Data Figure 6-1.

0.1858;  $p = 0.6698$ ; cortical side,  $F_{(1,28)} = 8.834$ ;  $p = 0.006$ ; interaction,  $F_{(1,28)} = 0.6357$ ;  $p = 0.432$ ) were significantly increased in the contralateral SSC of CFA-injected mice ( $p < 0.05$  vs the ipsilateral side), whereas the transcript encoding aggrecan (treatment,  $F_{(1,27)} = 2.38$ ;  $p = 0.1346$ ; cortical side,  $F_{(1,27)} = 0.0854$ ;  $p = 0.7723$ ; interaction,  $F_{(1,27)} = 4.569$ ;  $p = 0.0418$ ) was significantly reduced in the contralateral SSC of CFA-injected mice ( $p < 0.05$  vs the ipsilateral side). All other transcripts were

unchanged, although there was a trend to a decrease in the transcript encoding MMP-9 in the contralateral SSC (Fig. 6).

**Enzymatic degradation of PNNs in the contralateral SSC caused analgesia in CFA-injected mice**

PNNs have a structure similar to cartilage, in which anchoring proteins (Crtl1/Hapln1 and Bral2/Hapln4) stabilize the binding of various CSPGs to hyaluronan (Mörgelin et al., 1994;



Watanabe et al., 1998; Carulli et al., 2007). Digestion of CSPGs with the enzyme ChABC causes a marked reduction of PNNs around the cortex, although it also affects the diffuse extracellular matrix around neurons and glia (Pizzorusso et al., 2002; Gogolla et al., 2009). Thus, to examine the importance of the relationship between the build-up of PNNs and the development of nociceptive sensitization, we stereotaxically infused ChABC or its vehicle in three regions of the contralateral SSC (AP: 1.00; 0.00; and  $-1.00$  mm from bregma). ChABC infusion caused the disappearance of WFA<sup>+</sup> PNNs in the SSC (Fig. 7A,B) (WFA<sup>+</sup> PNNs: treatment,  $F_{(1,12)} = 129.1$ ,  $p < 0.0001$ ; side,  $F_{(1,12)} = 45.93$ ,  $p < 0.0001$ ; interactions,  $F_{(1,12)} = 169.8$ ,  $p < 0.0001$ ; WFA<sup>+</sup>/PV<sup>+</sup> cells: treatment,  $F_{(1,12)} = 179.1$ ,  $p < 0.0001$ ; side,  $F_{(1,12)} = 62.66$ ,  $p < 0.0001$ ; interactions,  $F_{(1,12)} = 171.00$ ,  $p < 0.0001$ ). Local infusions were performed 4 d after CFA injection, and mechanical thresholds were assessed at day 7 and compared with those obtained at day 4 (1 h before local infusions). Interestingly, mechanical thresholds at 7 d were significantly enhanced in mice injected with ChABC (Fig. 7C). No changes in mechanical thresholds were caused by infusion of vehicle (treatment,  $F_{(1,19)} = 16.003$ ,  $p < 0.001$ ; side,  $F_{(1,19)} = 69.775$ ,  $p < 0.001$ ; interactions,  $F_{(1,19)} = 1.218$ ,  $p = 0.283$ ) in the SSC (Fig. 7C). We performed additional experiments to examine the effect of PNN degradation on thermal pain in CFA-injected mice. As expected, CFA injection caused a significant reduction in thermal latencies in the hot plate test after 4 d (1 h before ChABC or vehicle infusion in the contralateral SSC). ChABC, but not vehicle, infusion significantly enhanced thermal latencies in CFA-injected mice (Fig. 7D) (treatment,  $F_{(1,10)} = 2.754$ ,  $p = 0.1280$ ; time,  $F_{(2,20)} = 73.13$ ,  $p < 0.0001$ ; interactions,  $F_{(2,20)} = 4.232$ ,  $p = 0.0293$ ). ChABC infusion had no effect on mechanical thresholds or thermal latencies in naive mice (i.e., in mice that were not injected with either CFA or vehicle in the hindpaw) (Fig. 7E,F).

### Relationship between PNNs and changes in inhibitory synaptic transmission in the contralateral SSC of mice with chronic pain

Knowing that PNNs preferentially enwrap GABAergic interneurons (see Introduction and references therein), we first examined whether CFA caused changes in inhibitory synaptic transmission in the SSC. We recorded sIPSCs from L5 pyramidal neurons, at 7 d after CFA or vehicle injection. IPSC frequency did not differ between the ipsilateral and contralateral SSC of

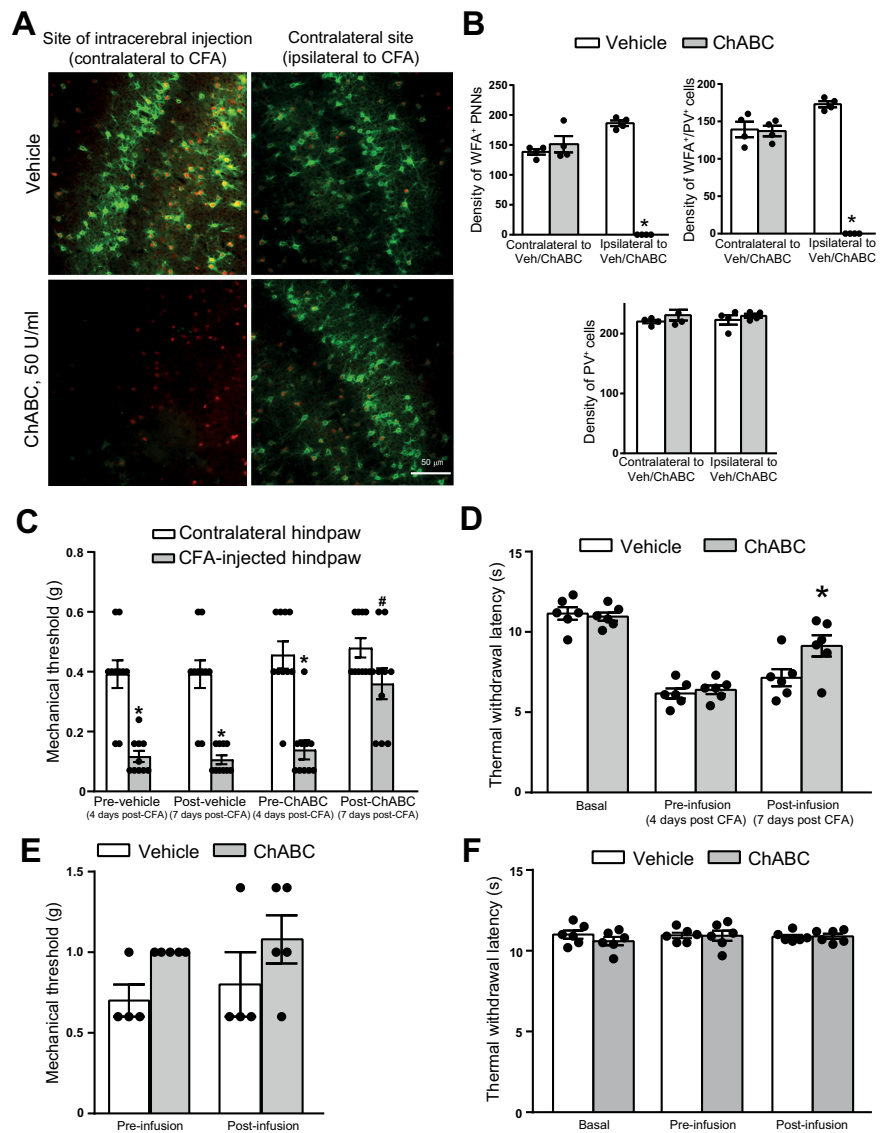


**Figure 7.** Enzymatic degradation of PNNs in the contralateral SSC caused analgesia in CFA-injected mice. **A**, The efficacy of ChABC (50 U/ml) in causing complete PNN degradation. Green represents WFA<sup>+</sup>/PNNs. Red represents PV<sup>+</sup> neurons. **B**, Bar graphs represent the density of WFA<sup>+</sup> PNNs, WFA<sup>+</sup>/PV<sup>+</sup> cells, or PV<sup>+</sup> cells. Values are mean ± SEM of 4 mice per group. \*Significantly different versus all other values. **C**, Mechanical pain thresholds of CFA-treated mice receiving either vehicle (0.1% BSA) or ChABC in the contralateral SSC. Thresholds were measured at day 4 following CFA injection (1 h before intracortical infusion with either vehicle or ChABC), and then at day 7 in the same mice. Values are mean ± SEM of 10 mice per group. Significantly different versus the respective values of the contralateral hindpaw (\*) or versus all other groups of CFA-injected hindpaw (#). **D**, Thermal pain latencies determined in additional groups of CFA-treated mice receiving either vehicle (0.1% BSA) or ChABC in the contralateral SSC. Values are mean ± SEM of 6 mice per group. Significantly different versus the respective thresholds measured before ChABC infusion (\*). The effect of intracortical ChABC infusion on mechanical and thermal pain in naive mice is shown in **E** and **F**, respectively. Values are mean ± SEM of 4 or 5 mice per group in **E**, and 6 mice per group in **F**.

control mice injected with vehicle in the hindpaw. A similar sIPSC frequency was found in 5 neurons recorded from the ipsilateral SSC of animal injected with CFA (Fig. 8A–C). In contrast, we found a significant increase in sIPSC frequency in 7 pyramidal neurons recorded from the contralateral SSC of CFA-injected mice treatment ( $F_{(1,19)} = 3.85$ ;  $p = 0.0646$ ; cortical side,  $F_{(1,19)} = 3.155$ ;  $p = 0.0917$ ; interaction,  $F_{(1,19)} = 3.199$ ;  $p = 0.0896$ ) (Fig. 8A–C). No changes in other kinetic parameters of GABAergic transmission were found in the contralateral cortex of CFA-injected mice (Extended Data Fig. 8-1A–E).

We also examined whether enzymatic degradation of PNNs could affect inhibitory synaptic transmission in mice



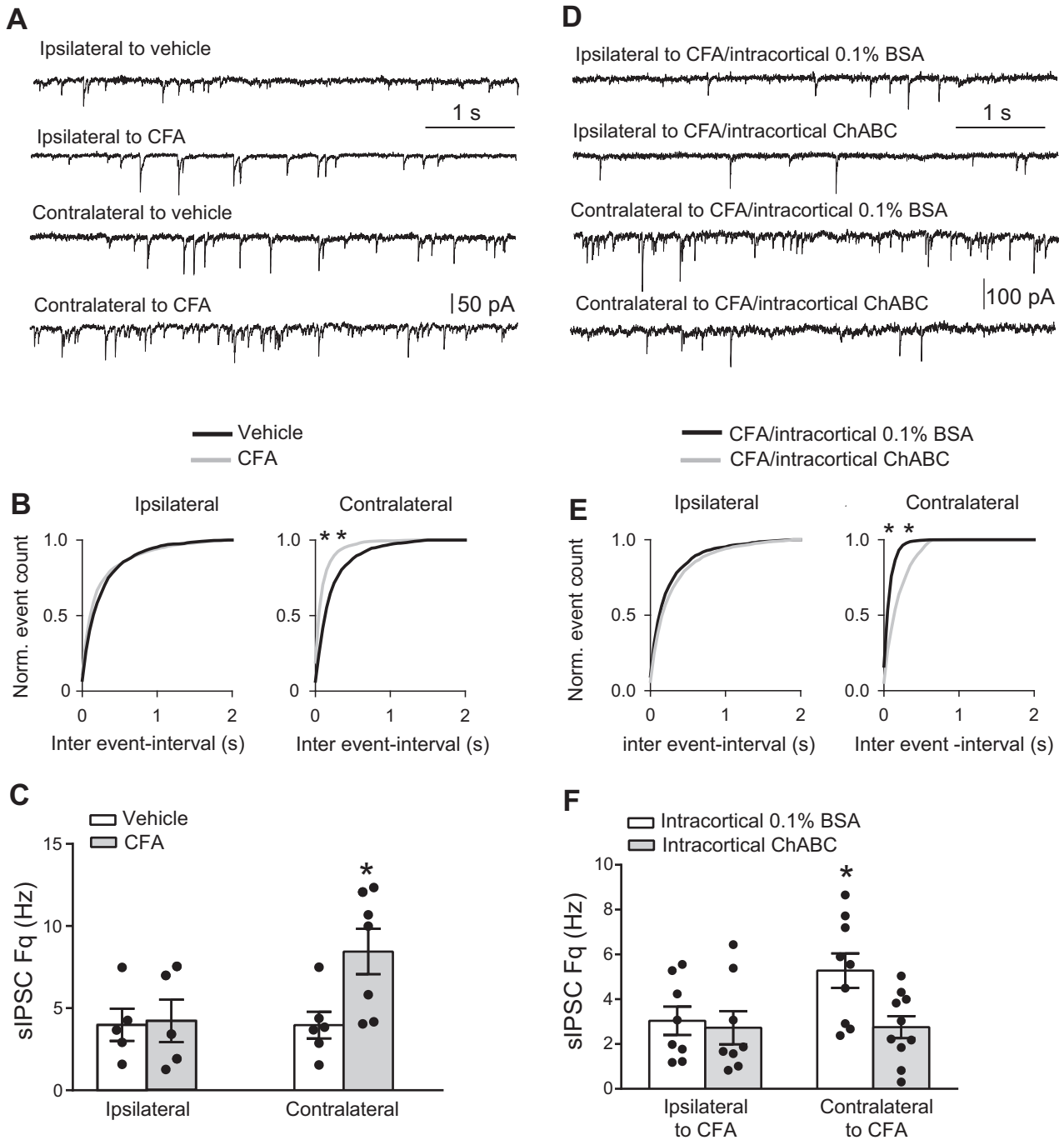


**Figure 8.** Enzymatic degradation of PNNs reverses abnormalities in inhibitory synaptic transmission in the SSC of mice with chronic pain. **A–C**, Increased sIPSC frequency in L5 pyramidal neurons of the contralateral SSC 7 d following CFA or vehicle injection. **A**, Representative traces. Cumulative distribution of interevent interval values in the SSC ipsilateral (left,  $p = 0.54$ ,  $K_s = 0.187$ ) or contralateral (right,  $**p < 0.001$ ;  $K_s = 0.875$ ) to CFA or vehicle injections are in **B**. **C**, Bar graphs represent the mean frequency values obtained from the same cells as in **B**.  $*p < 0.05$  versus the corresponding value of mice treated with vehicle. **D–F**, Local infusion of ChABC in the contralateral SSC reverses the increased frequency of sIPSCs in L5 pyramidal neurons of CFA-injected mice. **D**, Representative traces. **E**, Cumulative distribution of interevent interval values in the SSC ipsilateral (left,  $p = 0.256$ ;  $K_s = 0.237$ ) or contralateral (right,  $**p < 0.001$ ;  $K_s = 0.939$ ) to CFA injection after local infusion with either ChABC (50 U/ml) or 0.1% BSA. **F**, Bar graphs represent the mean frequency values in the same cells as in **E**.  $*p < 0.05$  versus the corresponding value of mice infused with 0.1% BSA. Kinetic parameters of sIPSCs are reported in Extended Data Figure 8-1.

with chronic pain. Local infusion of the ChABC vehicle (0.1% BSA in PBS) in the SSC contralateral to CFA injection did not change sIPSC frequency in mice with inflammatory pain. In contrast, intracortical ChABC infusion significantly reduced sIPSC frequency recorded on L5 pyramidal neurons (treatment,  $F_{(1,31)} = 4.561$ ;  $p = 0.0407$ ; cortical side,

$F_{(1,31)} = 2.933$ ;  $p = 0.0968$ ; interaction,  $F_{(1,31)} = 2.801$ ;  $p = 0.1043$ ) (Fig. 8D–F). All other parameters of GABAergic transmission were unaffected (Extended Data Fig. 8-1F–J).

These findings combined with the effect of ChABC infusion on pain thresholds (see above) suggested the possibility that enzymatic degradation of PNNs caused analgesia by

restraining inhibition at the synapses between GABAergic interneurons and pyramidal neurons in the SSC. However, this interpretation is limited by nonspecific effects of ECM degradation at all synapses of the SSC.

## Discussion

Our findings are consistent with the evidence that PNNs are dynamic structures in the adult brain, and may have a key role in mechanisms of neuronal plasticity in physiology and pathology (for review, see Carulli and Verhaagen, 2021). Interestingly, changes in PNNs have been associated to learning and memory processes. For example, the acquisition of auditory fear memory is associated with increases in PNN density in the auditory cortex, hippocampus, and cingulate cortex (Banerjee et al., 2017; Shi et al., 2019), and brevican content in PNNs surrounding PV<sup>+</sup> neurons is reduced in the hippocampus during learning acquisition in the Morris water maze (Favuzzi et al., 2017). Changes in PNNs have been associated with drug addiction (Lasek et al., 2018), which reflects a maladaptive form of neuronal plasticity (Koob and Volkow, 2016). Nociceptive sensitization is another form of maladaptive synaptic plasticity resulting in a reinforcement of pain signaling throughout the pain neuraxis, including the S1 SSC, which is involved in pain perception (Vierck et al., 2013), the mPFC, which has a key role in pain processing and encodes the emotional aspects of pain (Ong et al., 2019), and the RTN, which responds to nociceptive inputs and regulates sensitivity to pain (Olivéras and Montagne-Clavel, 1994; Ab Aziz and Ahmad, 2006; Huh and Cho, 2016; Liu et al., 2017). We have found significant increases in the density of WFA<sup>+</sup> PNNs in the primary SSC, mPFC, and RTN of mice developing chronic inflammatory pain in response to CFA injection in the hindpaw. This indicates that changes in PNNs may occur in different regions of the pain matrix, although the extent and kinetics of these changes were region-dependent. Accordingly, an increase in WFA<sup>+</sup>/PNN density could be demonstrated at both 3 and 7 d after CFA injection in the contralateral SSC, but only at 7 d in the contralateral mPFC (PNNs were exclusively examined at 7 d in the RTN). Most, but not all, WFA<sup>+</sup> PNNs we have detected enwrapped PV<sup>+</sup> interneurons, with quantitative differences among the three regions (see Results). Although the percentage of WFA<sup>+</sup>/PV<sup>+</sup> cells with respect to total WFA<sup>+</sup> PNNs increased or remained constant in CFA-injected mice, we cannot exclude that chronic inflammatory pain enhances the formation of PNNs surrounding other types of interneurons (e.g., somatostatin-expressing or caudal ganglionic eminence-derived interneurons), and this may have a role in nociceptive sensitization (see below).

Analysis of the transcripts encoding structural components or degrading enzymes of PNNs showed significant increases in NPTX2 and Tnr and a reduction in Acan mRNA levels in the contralateral SSC of CFA-injected mice. NPTX2 encodes Narp, a calcium-dependent lectin, which supports spontaneous firing of PV<sup>+</sup> interneurons (O'Brien et al., 1999; Chang et al., 2010). Narp binds to hyaluronan and chondroitin sulfate E, and is known to enhance PNN formation in cortical neurons (Van't Spijker et al., 2019). Tnr encodes tenascin-R, a CNS-specific member of tenascin family. A large body of evidence indicates that tenascin-R is essential for PNN development, and provides a molecular

scaffolding for lecticans (Lundell et al., 2004; Rathjen and Hodge, 2020). Interestingly, the transcript encoding the PNN structural component, aggrecan, which is physically linked to tenascin-R (Sorg et al., 2016), was reduced in the SSC of CFA-injected mice, suggesting, but not proving, that chronic pain induced structurally different PNNs. There was only a trend to a reduction in the transcript encoding MMP-9, a major PNN-degrading enzyme, which regulates the rigidity of extracellular matrix, and has been implicated in the early phases of neuropathic pain (Kawasaki et al., 2008).

An early increase in Narp expression (detected at 3 d following CFA injection) might contribute to the enhanced inhibitory synaptic transmission we have found in the contralateral SSC of CFA-injected mice 4 d later. PNN-associated Narp regulates synaptic scaling and AMPAR clustering in dendritic spines of PV<sup>+</sup> interneurons (Chang et al., 2010). Reductions in PNNs and associated Narp, as observed in mouse models of Fragile-X syndrome, impair the functioning of PV<sup>+</sup> interneurons, resulting in cortical hyperexcitability (Wen et al., 2018; Lovelace et al., 2020). We found an increased frequency of sIPSCs recorded in SSC pyramidal neurons of CFA-injected mice. To examine the possible relationship between PNN formation, enhancement of inhibitory synaptic transmission, and chronic inflammatory pain, we used the PNN-degrading enzyme, ChABC (Pizzorusso et al., 2002; Gogolla et al., 2009). We used an infusion protocol of ChABC that caused a large depletion of PNNs in the SSC, leaving the density of PV<sup>+</sup> interneurons unchanged. Remarkably, this treatment caused analgesia and reversed the enhanced synaptic inhibition of L5 pyramidal neurons associated with chronic pain. This suggests a potential scenario in which sustained painful stimuli induce the formation of NPAS4-containing PNNs, which enhance the activity of PV<sup>+</sup> interneurons by stabilizing their excitatory inputs (Carulli and Verhaagen, 2021). However, the hypothesis that an enhanced GABAergic transmission in the SSC supports nociceptive sensitization is in contrast with the evidence that pharmacological activation of cortical GABA<sub>A</sub> receptors relieves neuropathic pain, whereas receptor blockade induces pain (Olivéras and Montagne-Clavel, 1996; Eto et al., 2011, 2012). Experiments in which the activity of distinct types of GABAergic interneurons is selectively inhibited or amplified are required to better clarify the potential relationship between PNNs, inhibitory GABAergic transmission in the SSC, and chronic pain.

The pharmacology of PNNs is still at its infancy. We have shown that genetic deletion of mGlu5 receptors has a strong impact on PNN formation/degradation in the SSC (Mascio et al., 2021), raising the attractive possibility that PNNs are regulated by druggable targets. The search for systemic drugs that have a direct impact on PNN plasticity may pave the way to novel treatments for chronic pain.

## References

- Ab Aziz CB, Ahmad AH (2006) The role of the thalamus in modulating pain. *Malays J Med Sci* 13:11–18.
- Banerjee SB, Gutzeit VA, Baman J, Aoued HS, Doshi NK, Liu RC, Ressler KJ (2017) Perineuronal nets in the adult sensory cortex are necessary for fear learning. *Neuron* 95:169–179.e5.
- Berretta S (2012) Extracellular matrix abnormalities in schizophrenia. *Neuropharmacology* 62:1584–1597.
- Berretta S, Pantazopoulos H, Markota M, Brown C, Batzianouli ET (2015) Losing the sugar coating: potential impact of perineuronal

- net abnormalities on interneurons in schizophrenia. *Schizophr Res* 167:18–27.
- Beurdeley M, Spatzza J, Lee HH, Sugiyama S, Bernard C, Di Nardo AA, Hensch TK, Prochiantz A (2012) Otx2 binding to perineuronal nets persistently regulates plasticity in the mature visual cortex. *J Neurosci* 32:9429–9437.
- Bushnell MC, Duncan GH, Hofbauer RK, Ha B, Chen JI, Carrier B (1999) Pain perception: is there a role for primary somatosensory cortex? *Proc Natl Acad Sci USA* 96:7705–7709.
- Carulli D, Verhaagen J (2021) An extracellular perspective on CNS maturation: perineuronal nets and the control of plasticity. *Int J Mol Sci* 22:2434.
- Carulli D, Rhodes KE, Fawcett JW (2007) Upregulation of aggrecan, link protein 1, and hyaluronan synthases during formation of perineuronal nets in the rat cerebellum. *J Comp Neurol* 501:83–94.
- Chang MC, Park JM, Pelkey KA, Grabenstatter HL, Xu D, Linden DJ, Sutula TP, McBain CJ, Worley PF (2010) Narp regulates homeostatic scaling of excitatory synapses on parvalbumin-expressing interneurons. *Nat Neurosci* 13:1090–1097.
- Eto K, Wake H, Watanabe M, Ishibashi H, Noda M, Yanagawa Y, Nabekura J (2011) Inter-regional contribution of enhanced activity of the primary somatosensory cortex to the anterior cingulate cortex accelerates chronic pain behavior. *J Neurosci* 31:7631–7636.
- Eto K, Ishibashi H, Yoshimura T, Watanabe M, Miyamoto A, Ikenaka K, Moorhouse AJ, Nabekura J (2012) Enhanced GABAergic activity in the mouse primary somatosensory cortex is insufficient to alleviate chronic pain behavior with reduced expression of neuronal potassium-chloride cotransporter. *J Neurosci* 32:16552–16559.
- Favuzzi E, Marques-Smith A, Deogracias R, Winterflood CM, Sánchez-Aguilera A, Mantoan L, Maeso P, Fernandes C, Ewers H, Ricono B (2017) Activity-dependent gating of parvalbumin interneuron function by the perineuronal net protein brevicain. *Neuron* 95:639–655.e10.
- Gogolla N, Caroni P, Lüthi A, Herry C (2009) Perineuronal nets protect fear memories from erasure. *Science* 325:1258–1261.
- Hsieh TH, Lee HH, Hameed MQ, Pascual-Leone A, Hensch TK, Rotenberg A (2017) Trajectory of parvalbumin cell impairment and loss of cortical inhibition in traumatic brain injury. *Cereb Cortex* 27:5509–5524.
- Huh Y, Cho J (2016) Differential responses of thalamic reticular neurons to nociception in freely behaving mice. *Front Behav Neurosci* 10:223.
- Kawasaki Y, Xu ZZ, Wang X, Park JY, Zhuang ZY, Tan PH, Gao YJ, Roy K, Corfas G, Lo EH, Ji RR (2008) Distinct roles of matrix metalloproteases in the early- and late-phase development of neuropathic pain. *Nat Med* 14:331–336.
- Kim SK, Nabekura J (2011) Rapid synaptic remodeling in the adult somatosensory cortex following peripheral nerve injury and its association with neuropathic pain. *J Neurosci* 31:5477–5482.
- Kim SK, Eto K, Nabekura J (2012) Synaptic structure and function in the mouse somatosensory cortex during chronic pain: in vivo two-photon imaging. *Neural Plast* 2012:640259.
- Komagata S, Chen S, Suzuki A, Yamashita H, Hishida R, Maeda T, Shibata M, Shibuki K (2011) Initial phase of neuropathic pain within a few hours after nerve injury in mice. *J Neurosci* 31:4896–4905.
- Koob GF, Volkow ND (2016) Neurobiology of addiction: a neurocircuitry analysis. *Lancet Psychiatry* 3:760–773.
- Lasek AW, Chen H, Chen WY (2018) Releasing addiction memories trapped in perineuronal nets. *Trends Genet* 34:197–208.
- Letremoliere A, Woolf CJ (2009) Central sensitization: a generator of pain hypersensitivity by central neural plasticity. *J Pain* 10:895–926.
- Liu J, Zhang MQ, Wu X, Lazarus M, Cherasse Y, Yuan MY, Huang ZL, Li RX (2017) Activation of parvalbumin neurons in the rostro-dorsal sector of the thalamic reticular nucleus promotes sensitivity to pain in mice. *Neuroscience* 366:113–123.
- Lovelace JW, Rais M, Palacios AR, Shuai XS, Bishay S, Popa O, Pirbhoy PS, Binder DK, Nelson DL, Ethell IM, Razak KA (2020) Deletion of Fmr1 from forebrain excitatory neurons triggers abnormal cellular, EEG, and behavioral phenotypes in the auditory cortex of a mouse model of Fragile X syndrome. *Cereb Cortex* 30:969–988.
- Lundell A, Olin AI, Mörgelein M, al-Karadaghi S, Asperg A, Logan DT (2004) Structural basis for interactions between tenascins and lectican-C-type lectin domains: evidence for a crosslinking role for tenascins. *Structure* 12:1495–1506.
- Martinello K, Sciacaluga M, Morace R, Mascia A, Arcella A, Esposito V, Fucile S (2018) Loss of constitutive functional  $\gamma$ -aminobutyric acid type A-B receptor crosstalk in layer 5 pyramidal neurons of human epileptic temporal cortex. *Epilepsia* 59:449–459.
- Mascio G, Bucci D, Notartomaso S, Liberatore F, Antenucci N, Scarselli P, Imbriglio T, Caruso S, Gradini R, Cannella M, Di Menna L, Bruno V, Battaglia G, Nicoletti F (2021) Perineuronal nets are under the control of type-5 metabotropic glutamate receptors in the developing somatosensory cortex. *Transl Psychiatry* 11:109.
- Miyata S, Komatsu Y, Yoshimura Y, Taya C, Kitagawa H (2012) Persistent cortical plasticity by upregulation of chondroitin 6-sulfation. *Nat Neurosci* 15:414–422.
- Mörgelein M, Heinegård D, Engel J, Paulsson M (1994) The cartilage proteoglycan aggregate: assembly through combined protein-carbohydrate and protein-protein interactions. *Biophys Chem* 50:113–128.
- O'Brien RJ, Xu D, Petralia RS, Steward O, Haganir RL, Worley P (1999) Synaptic clustering of AMPA receptors by the extracellular immediate-early gene product Narp. *Neuron* 23:309–323.
- Olivéras JL, Montagne-Clavel J (1994) The GABA receptor antagonist picrotoxin induces a 'pain-like' behavior when administered into the thalamic reticular nucleus of the behaving rat: a possible model for 'central' pain? *Neurosci Lett* 179:21–24.
- Olivéras JL, Montagne-Clavel J (1996) Picrotoxin produces a 'central' pain-like syndrome when microinjected into the somato-motor cortex of the rat. *Physiol Behav* 60:1425–1434.
- Ong WY, Stohler CS, Herr DR (2019) Role of the prefrontal cortex in pain processing. *Mol Neurobiol* 56:1137–1166.
- Paxinos G, Franklin KB (2001) The mouse brain in stereotaxic coordinates. San Diego: Academic.
- Pizzorusso T, Medini P, Berardi N, Chierzi S, Fawcett JW, Maffei L (2002) Reactivation of ocular dominance plasticity in the adult visual cortex. *Science* 298:1248–1251.
- Potter LE, Paylor JW, Suh JS, Tenorio G, Caliaperumal J, Colbourne F, Baker G, Winship I, Kerr BJ (2016) Altered excitatory-inhibitory balance within somatosensory cortex is associated with enhanced plasticity and pain sensitivity in a mouse model of multiple sclerosis. *J Neuroinflammation* 13:142.
- Rathjen FG, Hodge R (2020) Early days of tenascin-R research: two approaches discovered and shed light on tenascin-R. *Front Immunol* 11:612482.
- Rivera C, Voipio J, Payne JA, Ruusuvaari E, Lahtinen H, Lamsa K, Pirvola U, Saarna M, Kaila K (1999) The  $K^+/Cl^-$  co-transporter KCC2 renders GABA hyperpolarizing during neuronal maturation. *Nature* 397:251–255.
- Shi W, Wei X, Wang X, Du S, Liu W, Song J, Wang Y (2019) Perineuronal nets protect long-term memory by limiting activity-dependent inhibition from parvalbumin interneurons. *Proc Natl Acad Sci USA* 116:27063–27073.
- Slaker M, Churchill L, Todd RP, Blacktop JM, Zuloaga DG, Raber J, Darling RA, Brown TE, Sorg BA (2015) Removal of perineuronal nets in the medial prefrontal cortex impairs the acquisition and reconsolidation of a cocaine-induced conditioned place preference memory. *J Neurosci* 35:4190–4202.
- Sorg BA, Berretta S, Blacktop JM, Fawcett JW, Kitagawa H, Kwok JC, Miquel M (2016) Casting a wide net: role of perineuronal nets in neural plasticity. *J Neurosci* 36:11459–11468.
- Takesian AE, Hensch TK (2013) Balancing plasticity/stability across brain development. *Prog Brain Res* 207:3–34.
- Testa D, Prochiantz A, Di Nardo AA (2019) Perineuronal nets in brain physiology and disease. *Semin Cell Dev Biol* 89:125–135.
- Tremblay R, Lee S, Rudy B (2016) GABAergic interneurons in the neocortex: from cellular properties to circuits. *Neuron* 91:260–292.
- Van't Spijker HM, Rowlands D, Rossier J, Haenzi B, Fawcett JW, Kwok JC (2019) Neuronal pentraxin 2 binds PNNs and enhances PNN formation. *Neural Plast* 2019:6804575.
- Vierck CJ, Whitsel BL, Favorov OV, Brown AW, Tommerdahl M (2013) Role of primary somatosensory cortex in the coding of pain. *Pain* 154:334–344.



- Watanabe H, Yamada Y, Kimata K (1998) Roles of aggrecan, a large chondroitin sulfate proteoglycan, in cartilage structure and function. *J Biochem* 124:687–693.
- Watanabe T, Sasaki M, Komagata S, Tsukano H, Hishida R, Kohno T, Baba H, Shibuki K (2015) Spinal mechanisms underlying potentiation of hindpaw responses observed after transient hindpaw ischemia in mice. *Sci Rep* 5:11191.
- Wen TH, Afroz S, Reinhard SM, Palacios AR, Tapia K, Binder DK, Razak KA, Ethell IM (2018) Genetic reduction of matrix metalloproteinase-9 promotes formation of perineuronal nets around parvalbumin-expressing interneurons and normalizes auditory cortex responses in developing *Fmr1* knock-out Mice. *Cereb Cortex* 28:3951–3964.
- Woolf CJ (1994) A new strategy for the treatment of inflammatory pain: prevention or elimination of central sensitization. *Drugs* 47 Suppl 5:1–47.
- Woolf CJ (2011) Central sensitization: implications for the diagnosis and treatment of pain. *Pain* 152:S2–S15.
- Woolf CJ, Salter MW (2000) Neuronal plasticity: increasing the gain in pain. *Science* 288:1765–1769.
- Woolf CJ, Walters ET (1991) Common patterns of plasticity contributing to nociceptive sensitization in mammals and *Aplysia*. *Trends Neurosci* 14:74–78.
- Xue YX, Xue LF, Liu JF, He J, Deng JH, Sun SC, Han HB, Luo YX, Xu LZ, Wu P, Lu L (2014) Depletion of perineuronal nets in the amygdala to enhance the erasure of drug memories. *J Neurosci* 34:6647–6658.